IEEE Access
Multidisciplinary | Rapid Review | Open Access Journal

Received July 18, 2021, accepted August 21, 2021, date of publication August 24, 2021, date of current version September 1, 2021.

Digital Object Identifier 10.1109/ACCESS.2021.3107605

A Triple-Band Dual-Open-Ring High-Gain High-Efficiency Antenna for Wearable Applications

TU TUAN LE, YONG-DEOK KIM, AND TAE-YEOUL YUN, (Member, IEEE)
Department of Electronic Engineering, Hanyang University, Seoul 133-791, South Korea

Corresponding author: Tae-Yeoul Yun (taeyeoul@hanyang.ac.kr)

This work was supported in part by the National Research Foundation of Korea under Grant 2018R1A5A7025522.

ABSTRACT This paper presents a triple-band open-ring high-gain high-efficiency antenna for 2.45/3.0/3.45 GHz wearable applications. The proposed antenna operates at 2.45 GHz for Industrial, Specific, and Medical (ISM) applications, 3.0 GHz for military applications, and 3.45 GHz for Worldwide Interoperability for Microwave Access (WiMAX) applications. The proposed triple-band antenna has excellent features for off-body communication, which has directional radiation pattern, high gain, high efficiency, low-specific absorption rate (SAR), and comfortability for wearers. In order to attain these features, the antenna structure consists of two substrates, a rigid substrate and a textile substrate. Two open-ring radiators and a 1 by 2 power divider feeding network are printed on a low-loss rigid substrate. In addition, a square conductive textile is adhered on the backside of the textile substrate. The open-ring radiator generates triple-band at 2.45, 3.0, and 3.45 GHz, in which the inner open-ring excites two resonant modes at high frequencies of 3.0 and 3.45 GHz. The outer open-ring excites a single resonant mode at a low frequency of 2.45 GHz. The outer annular ring is shorted to the ground plane by a shorting pin to miniaturize the antenna size and additionally maintain antenna stability. The conductive textile works as a full-ground plane or protective shield to reduce the electromagnetic waves toward the human body. Therefore, the SARs are significantly minimized. The compatibility of the proposed antenna for off-body communication is verified by measuring the antenna performance in free-space and on phantom/human bodies. The simulated and measured results show very good agreement.

INDEX TERMS Off-body, SAR, triple-band, flexible substrate, wearable antenna.

I. INTRODUCTION

Recently, wearable antennas for off-body communication have been drawing tremendous attention. They have been widely applied in various applications in modern life such as physical training, tracking soldiers in the military, healthcare, and activity monitoring systems. As a key component of these applications, wearable antennas are used to transfer the collected data from on-body sensors to external devices or databases. These applications require antennas with a compact size, high gain, high efficiency, directional radiation pattern, low specific absorption rate (SAR), and that provide comfortability to wearers. Various single-band antennas [1]–[11] have been reported for off-body communication. Among these antennas, broadband antennas [8]–[11] are preferable for implementing multiple function applications. In [8], a ring-shaped monopole is printed on the top surface of a jeans material substrate, which covers ultra-wideband (UWB) applications. Similarly, an UWB elliptical-shaped monopole antenna is proposed in [9]. In [10] and [11], planar inverted-F antenna (PIFA) antennas with dual resonance modes cover the entire 5 GHz wireless local-area network (WLAN) application. The abovementioned wearable antennas have wideband characteristics. However, one of the inherent drawbacks of the wide bandwidth is interference with other wireless systems.

To tackle this issue, numerous studies addressing dual-band wearable antennas have recently been presented [12]–[14]. In [12], a patch antenna is placed over metasurface structures with a composite right-left hand transmission line, which can generate dual-band modes with similar radiation properties. In [13], two parallel horizontal slots

The associate editor coordinating the review of this manuscript and approving it for publication was Hussein Attia.

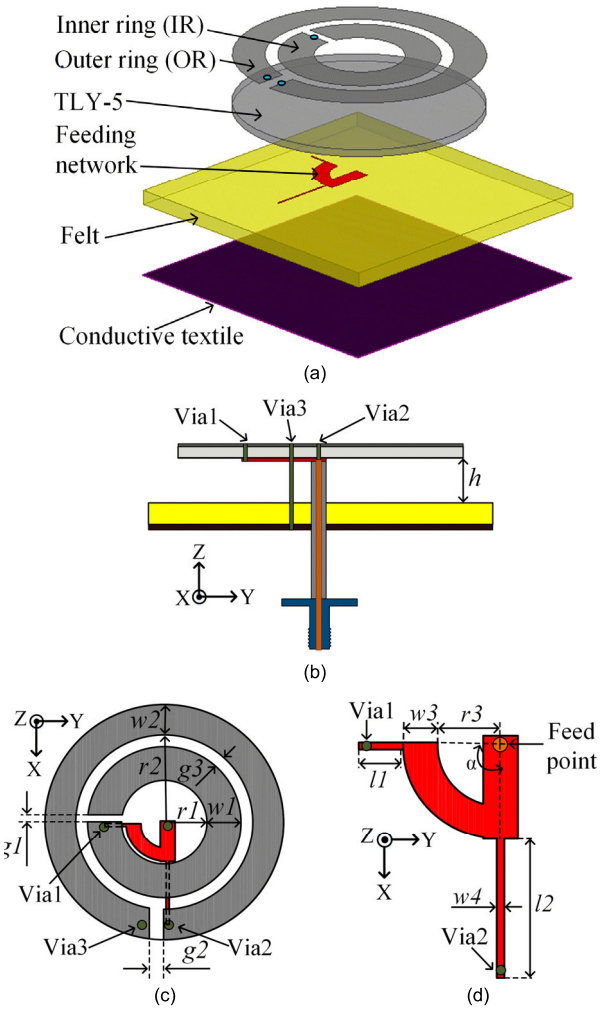

FIGURE 1. Geometry of the proposed antenna in: (a) perspective view, (b) side view, (c) top view, and (d) bottom view of the rigid substrate.

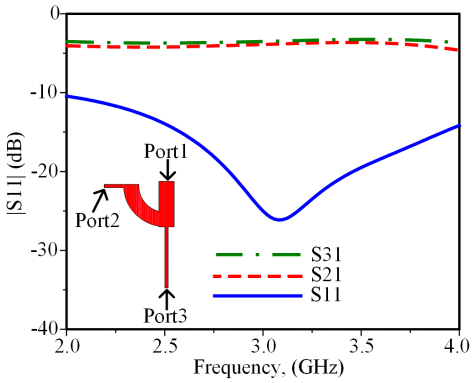

FIGURE 2. Simulated *S*-parameters of the feeding network.

and two verticals etched on a triangular-shaped monopole is proposed. Meanwhile in [14], a quarter-wavelength open-ended slot is etched into a quadrant circular microstrip antenna to realize dual-band characteristics. To further increase the number of bands, a method of using two Landolt ring-shaped strips connected by a rectangular strip and symmetrical stubs extended from the coplanar waveguide ground plane is proposed in [15], which achieves triple-bands. However, the rigid FR4 substrate adopted is not suitable for wearable application scenarios. To address this issue, other triple-band wearable antennas utilizing flexible substrate are presented in [16] and [17]. In [16], a substrate integrated waveguide (SIW) antenna based leather substrate is presented. The triple-band characteristic and antenna size miniaturization are implemented by introducing two slits into the tri-angular patch. However, this design suffers relatively low peak-gain of 1.1, 0.9, and 2.1 dB. In [17], another wearable antenna based jean substrate is designed, which yields wide triple-operating bandwidth. However, the other antenna parameters of gain, efficiency, and SAR are not detail mentioned. One of the drawback of the flexible substrate including textile, leather is having high loss tangent, which degrades the antenna performance. Therefore, a wearable triple-band button antenna with a 0.2 mm-thin low-loss tangent Rogers RO4003 is proposed in [18]. This antenna is featured by compact size, high gain, and high efficiency but two out of three bands with a limited bandwidth (BW) of less than 3%.

In this paper, a triple-band antenna with excellent features including high-gain, high-efficiency, and low SAR is proposed for ISM, military, and WiMAX applications. By implementing a combination of rigid and textile substrates on the antenna structure, the proposed antenna has excellent performance with/without the human body, but also comfortability for wearers. Two open-ring radiators, inner and outer rings as the main radiators, are printed on the low-loss rigid substrate to achieve high antenna performance. The triple-band characteristic of the proposed antenna is implemented by combining resonant modes of the inner ring and outer ring. A square conductive textile is attached on the textile substrate to avoid electromagnetic wave radiation toward the human body and to provide comfortability to wearers. The numerical simulations and the experimental results show very good agreement.

II. DESIGN OF THE ANTENNA

A. ANTENNA GEOMETRY AND FEEDING NETWORK

The geometry of the proposed wearable triple-band open-ring antenna for off-body communications is shown in Fig. 1. The proposed antenna structure consists of two substrates: a TLY-5 substrate and a felt substrate. Two open-ring radiators are printed on a Taconic TLY-5 substrate with a dielectric constant of 2.2, a loss tangent of 0.0009, and a thickness of 1.52 mm. The inner open-ring radiator, denoted as IR, has an inner radius and width of *r1* and *w1*, respectively. The inner radius and width of the outer open-ring radiator, denoted as OR, are *r2* and *w2*, respectively. The gaps on and between IR and OR are *g1*, *g2*, and *g3*. The gap directions on IR and OR are perpendicular to each other as shown in Fig. 1 (c).

A 1 2 feeding network [19] is printed on the backside of the TLY-5 substrate. The 90° (α) sector of the feeding

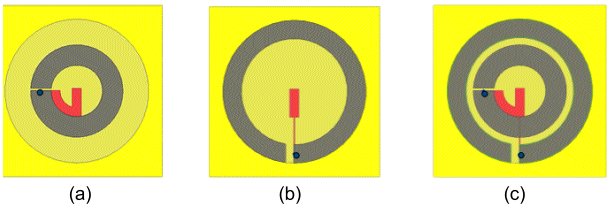

FIGURE 3. Investigation of antenna topologies: (a) Ant1, (b) Ant2, and (c) Ant3.

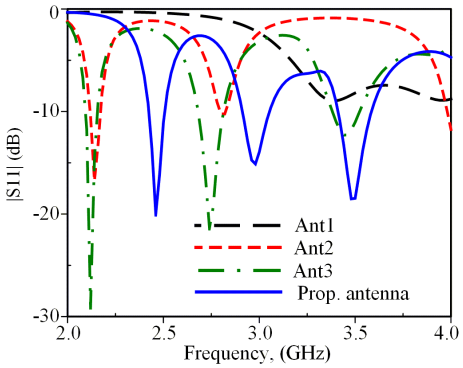

FIGURE 4. Simulated S_{11} to show the operating principle of the proposed antenna.

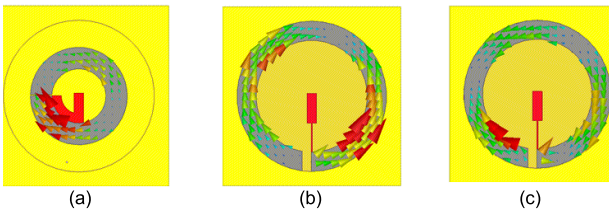

FIGURE 5. Simulated current distribution on inner and outer ring radiators at: (a) 3.4 GHz, (b) 2.1 GHz, and (c) 2.8 GHz.

network is printed inside the inner radius of IR observed from the $+z$ direction to mitigate the distortion to the IR radiation as shown in Fig. 1 (c). The feeding network is composed of a 90° sector and two output strips. A 50-Ω co-axial cable is soldered at the input power of the feeding network. Meanwhile, the output powers are delivered to IR and OR by two vias, Via1 and Via2, respectively. The feeding network sector has the inner radius of *r3* and width of *w3*. The width and lengths of the two output strips are *w4*, *l1*, and *l2* as shown in Fig. 1 (d). The feeding network provides IR and OR with balanced signals of equal magnitude. In addition, it transfers the impedance of IR and OR to match with the 50-Ω coaxial line at the input signal (Port1). The width of the 90° sector and the two extended strips are designed and optimized around 3.0 GHz as shown in Fig. 2. The reflection coefficient $S_{11} < -10$ dB of the power divider at Port1 ranges from 2 - 4 GHz. Meanwhile, the output powers have equal magnitude with the transmission coefficients S_{21} and S_{31} achieved of -3.5 ± 0.5 dB.

The ground plane is made of a ShielditTM super conductive textile with a conductivity of 11800 S/m on a felt

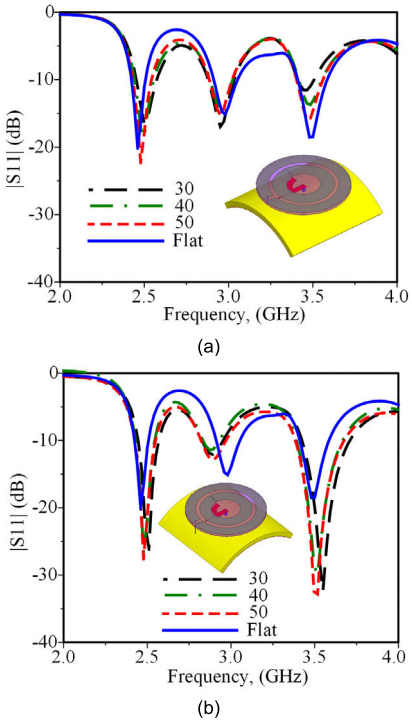

FIGURE 6. Bending effect of the proposed antenna in the (a) x-direction and (b) y-direction.

substrate with a thickness of 3 mm and a width of *ws*. The OR is shorted to the ground plane by a shorting pin, denoted as Via3, with a radius of 1 mm. Via3 also works as a supporter that maintains the spacing from the Taconic substrate to the felt substrate of *h*.

The antenna was characterized using the ANSYS high-frequency structure simulator (HFSS). The optimized geometrical parameters are listed as follows: $ws = 60$, $r1 = 9$, $w1 = 7.2$, $r2 = 18.7$, $w2 = 6.5$, $g1 = 0.4$, $g2 = 3$, $g3 = 2.5$, $r3 = 5.5$, $w3 = 3.5$, $l1 = 13$, $l2 = 3.6$, $w4 = 0.5$, $h = 3$ (unit: mm).

B. OPERATING PRINCIPLE

To understand the operating principle of the proposed antenna, three other antenna topologies; inner-ring only (Ant1), outer-ring only (Ant2), and the proposed antenna without Via3 (Ant3) are investigated as shown in Fig. 3. Note that the Ant1-3's parameters are kept the same as in the proposed design.

Ant1 is made of the IR, which operates as a half-wavelength antenna. The ring excites a fundamental mode TM_{11} at 3.4 GHz as shown in Fig. 5 (a). While, the gap excites a higher mode around 4.0 GHz as shown in Fig. 4 [20]. Similar to Ant1, Ant2 (which is made of OR) excites a fundamental mode TM_{11} around 2.1 GHz as shown in Fig. 5 (b) and a $TM_{1.5,1}$ half-mode at 2.8 GHz as shown in Fig. 5 (c). Ant3 combines Ant1 and Ant2 by the 1:2 feeding network. As can be observed in Fig. 4, Ant3 excites three resonant modes at 2.1, 2.8, and 3.5 GHz. The higher resonant

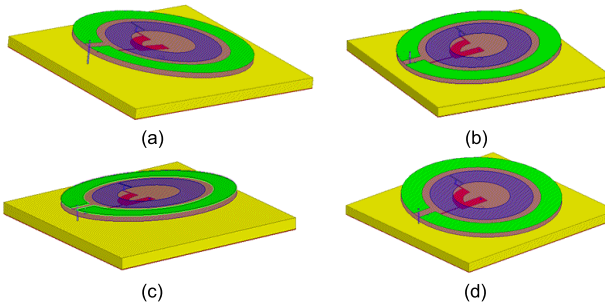

FIGURE 7. Proposal antenna with four tilting conditions including: (a) tilting back, (b) tilting front, (c) tilting left, and (d) titling right.

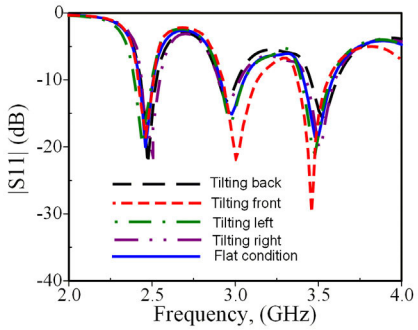

FIGURE 8. Simulated S_{11} in flat condition and different tilting conditions.

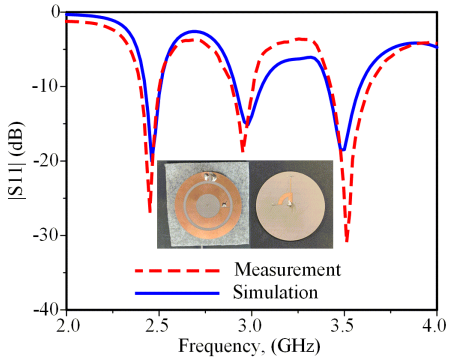

FIGURE 9. Simulated and measured S_{11} in free space.

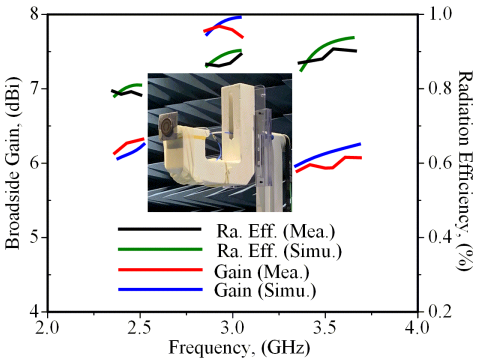

FIGURE 10. Simulated and measured broadside gains and radiation efficiencies in free space.

mode of Ant1 is shifted out of the considered band, which is not shown in Fig. 4. The resonant modes of Ant3 are slightly different from Ant1 and Ant2. The IR and OR radiate at different frequencies. When one radiates, the other can be treated as a load rather than a radiator. Therefore, the input impedance of a radiating ring at the feed point is affected by the position of the un-radiating ring behaving as a load, which is determined by $l1$, $l2$, and α [21].

To reduce the size of the antenna, a method of using a shorting pin (Via3) to provide additional inductance to the antenna structure [22] is adopted in Ant3, which produces the proposed antenna. In addition, Via3 can maintain the mechanical stability of the proposed antenna. As a result, the resonant modes, which are excited by OR, move from 2.1 to 2.45 GHz and from 2.75 to 3.0 GHz as shown in Fig. 4. Finally, the proposed antenna achieves resonant modes of 2.45, 3.0, and 3.45 GHz.

C. DEFORMATION STUDY

In some practical situations, the antenna is mounted on different parts of human body with different curvature surfaces. In addition, due to the movement of human body, the antenna might tilt into the different directions. This section is carried out to investigate the antenna performances for both bending and tilting condition.

Firstly, the proposed antenna is tested for the bending condition along a cylinder with a radius of R in the x- and y- directions. The simulated results with bending radius R of 30, 40, and 50 mm compared to the flat condition are shown in Fig. 6.

It is noted that a negligible frequency shift is observed for bending in the x-direction for all the bending radius cases. Meanwhile for bending in the y-direction, a slight frequency shift is observed at the middle band of 3.0 GHz. This phenomenon occurs because the OR has symmetrical structure in the x-direction but not in y-direction. Nevertheless, the resonant modes at 2.5 and 3.5 GHz for both x- and y- directions are maintained as in the flat condition.

In the tilting condition, four tilting situations are considered including tilting to the back, front, left, and right as shown in Fig. 7. Tilting angle of 5° is selected for investigation. As a result, the second and third bands are somewhat affected as shown in Fig. 8. However, the proposed antenna is still well covering the ISM, military, and WiMAX bands. In summary, the proposed antenna can work well under bending or tilting condition.

III. MEASUREMENT RESULTS

To validate the simulated results and confirm the suitability of the proposed antenna for off-body communications, the antenna is fabricated and then measured in free space and on human/phantom bodies.

A. FREE SPACE PERFORMANCE

The simulated and measured S_{11} in free space is shown in Fig. 9. The measured bandwidths of S_{11}

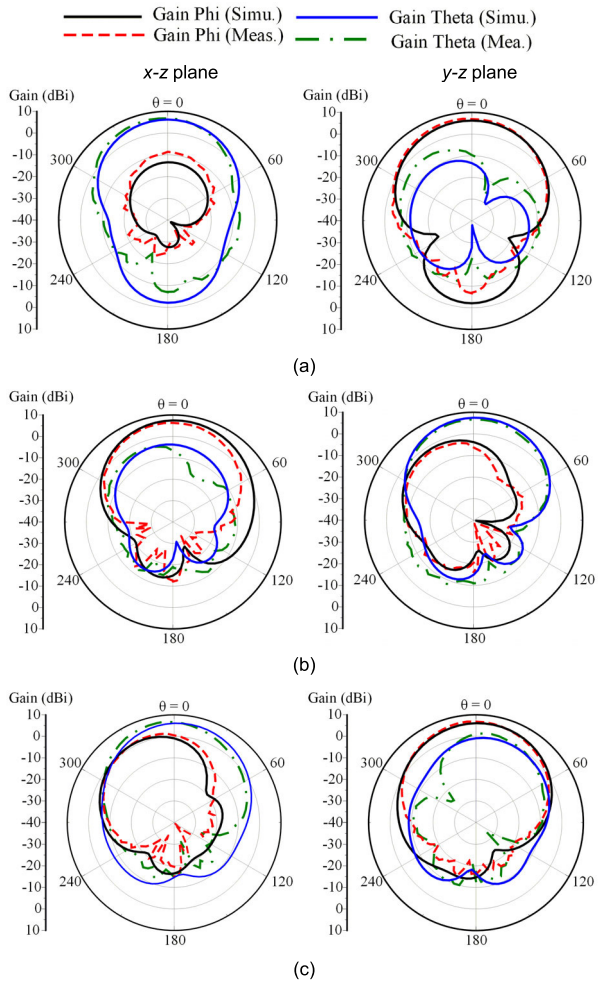

FIGURE 11. Simulated and measured radiation patterns in free space at (a) 2.45 GHz, (b) 3.0 GHz, and (c) 3.45 GHz.

are 4.48% (2.40-2.51 GHz), 4.05% (2.90-3.02), and 6.25% (3.41-3.63 GHz), similar to the simulated results of 3.65% (2.42-2.51 GHz), 4.69% (2.91-3.05 GHz), and 5.14% (3.41-3.59 GHz).

The measured broadside gain and radiation efficiency compared to the simulated results are presented in Fig. 10. The measured gains achieved at 2.45, 3.0, and 3.45 GHz are 6.2, 7.8, and 5.8 dBi, respectively. Meanwhile, the simulated results achieved are 6.14, 7.95, and 6.0 dBi, respectively. The measured radiation efficiencies are 77, 86, and 88%, which agree well with the simulated results of 80, 91, and 92%, respectively.

The simulated and measured radiation patterns in free space in the *x*-*z* and *y*-*z* planes at 2.45, 3.0, and 3.45 GHz are plotted in Fig. 11. The measured results indicate that the proposed antenna has directional radiation pattern, which is suitable for off-body communication. The measured front-to-back ratios (FBR) in the broadside direction at 2.45, 3.0, and 3.45 GHz are 9.2, 19, and 16.5 dB, respectively. Meanwhile, the measured cross polarization discriminations in the broadside direction are 20, 11, and 7 dB at 2.45, 3.0, and

TABLE 1. Human tissue.

Layer	Permittivity	Conductivity	Mass Density
Skin	35.11	3.72	1100
Fat	4.95	0.29	910
Muscle	48.48	4.96	1041

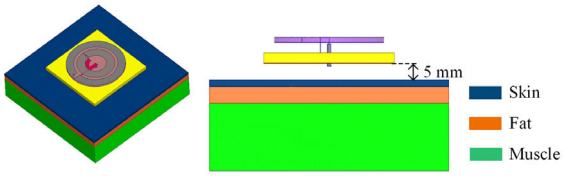

FIGURE 12. The model of three-layered human tissue.

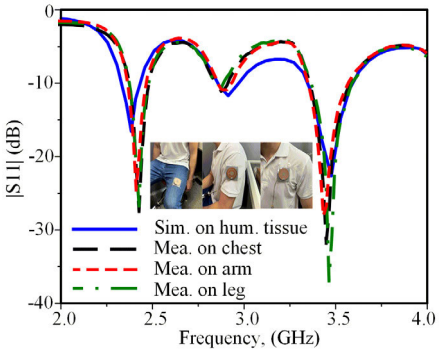

FIGURE 13. Simulated and measured S_{11} of the proposed antenna on different parts of the human body.

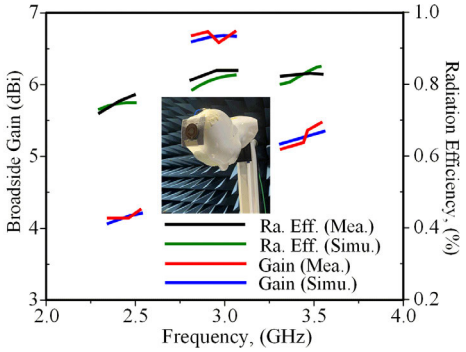

FIGURE 14. Simulated and measured broadside gains and radiation efficiencies on the human phantom.

3.45 GHz, respectively. The low cross polarization levels at 3.0 and 3.45 GHz are due to the asymmetric current distribution on the IR and OR as shown in Fig. 5 (a) and (c). The cross polarization behavior can be further improved by loading the open-end stubs or the parasitic elements. The simulated and measured results are well agreed.

B. ON BODY PERFORMANCE

In this section, the antenna performances with the presence of a human body or a human body-like environment

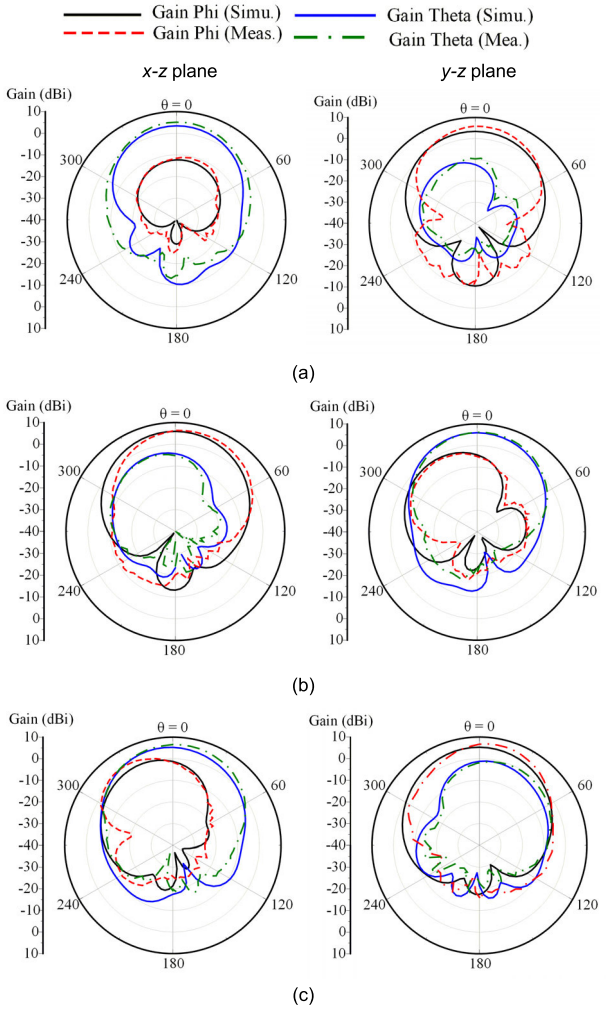

FIGURE 15. Simulated and measured radiation patterns of the proposed antenna on the human phantom at (a) 2.45 GHz, (b) 3.0 GHz, and (c) 3.45 GHz.

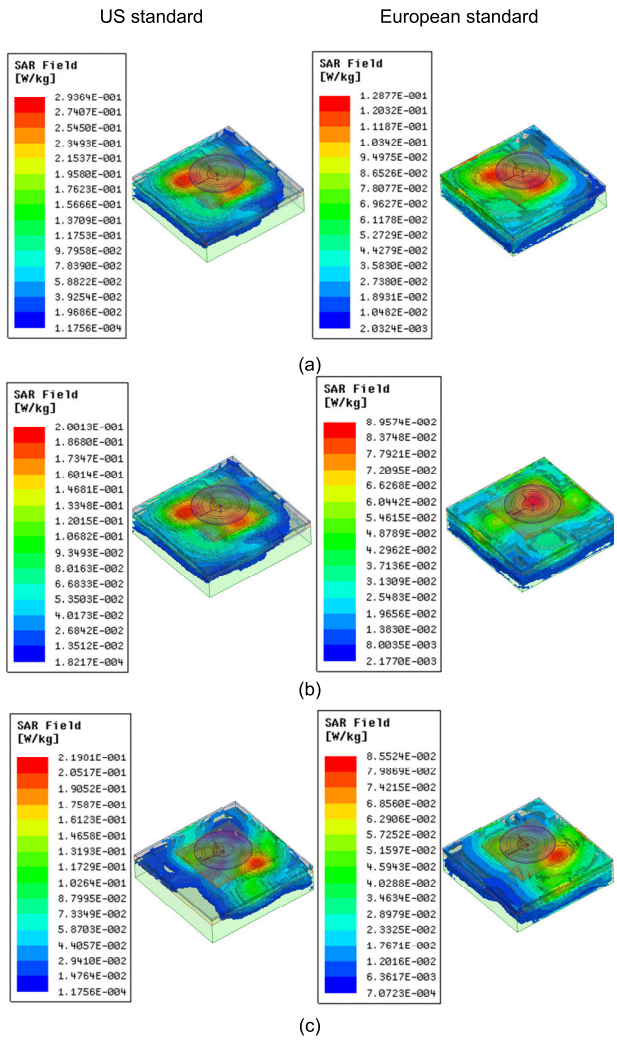

FIGURE 16. Simulated SAR for US and European standáards at (a) 2.45, (b) 3.0, and (c) 3.45 GHz.

are performed. To mimic a realistic situation, the proposed antenna is simulated over a 160 × 160 × 27 mm^3 three-layered human tissue sample as shown in Fig. 12, where the spacing distance from the proposed antenna to the human tissue is 5 mm. The three-layered tissue includes a 2 mm-thick skin, a 5 mm-thick fat, and a 20 mm-thick muscle. The details of relative permittivity, conductivity, and mass density are listed in Table 1.

Fig. 13 shows the comparison of the simulated and the measured S_{11} on different parts of the human body, including the chest, arm, and leg. The measured bandwidths of S_{11} achieved on the human arm representatively are 4.8% (2.43-2.55 GHz), 1.4% (2.94-2.98 GHz), and 6.2% (3.43-3.65 GHz), compared to the simulated S_{11} on human tissue of 4.44% (2.42-2.53 GHz), 2.6% (2.94-3.02 GHz), and 6.49% (3.43-3.66 GHz). It can be observed that the measured S_{11} in different parts of the human body are significantly consistent and in good agreement with the simulated results, except for a slight difference at the first and second resonant band. This may be caused by inaccurate alignment of the rigid and textile substrates in the fabrication process.

The simulated and measured gains in the broadside direction and the radiation efficiencies on the human phantom are shown in Fig. 14. The measured broadside gains are 4.2, 6.6, and 5.5 dB, and the measured radiation efficiencies are 79, 83, and 82% at 2.45, 3.0, and 3.45 GHz, respectively. Both measured results well agree with the simulated ones. The measured gain and radiation efficiencies on the human phantom are slightly deteriorated compared to the measured results in free space.

The simulated and measured radiation patterns of the proposed antenna on the human phantom in the *x*-*z* and *y*-*z* planes at 2.45, 3.0, and 3.45 GHz are shown in Fig. 15. The measured FBRs achieved at 2.45, 3.0, and 3.45 GHz are 14.5, 22.5, and 20.3 dB, respectively. Meanwhile, the measured cross-polarization discriminations are 16, 10.5, and 7 dB, respectively. The simulated and measured results well agree. It is noted that there are slight differences between the measured results in free space and on the human body or the phantom body environments. The differences are caused by the human proximity effect and the bending of the

TABLE 2. Comparison with other triple-band antennas for wearable applications.

Ref	BW (%)	f_0 (GHz)	Overall Size (λ^3_0)	Gain (dBi)	Efficiency (%)	SAR (W/kg)	Substrate
[15]	35.5/4.2/34.1	3.5/5.5/9.1	0.44 × 0.33 × 0.02	3.09/2.8/5.05	41/42/49	N.A	FR4
[16]	11/7/5	2.4/3.5/4.6	0.67 × 0.67 × 0.02	1.1/0.9/2.1	71/68/76	N.A	Leather
[17]	23.3/56.4/31.1	3.9/6.5/12.2	0.3 × 0.3 × 0.01	4.85/N.A/N.A	N.A/N.A/N.A	N.A/1.8/N.A	Jean
[18]	4.3/2.1/2.5	0.8/2.3/5.8	0.05 × 0.05 × 0.0006	2.5/3.52/4.8	78/85/89	0.26/0.57/0.93	Rogers
This work	4.4/4.0/6.2	2.45/3.0/3.45	0.5 × 0.5 × 0.06	4.2/6.6/5.0	79/83/82	0.13/0.09/0.09*	TLY-5/Felt

λ_0 : at lowest resonant frequency

*: SAR value for European standard

ground plane on the phantom body during the measurement process.

C. SAR ANALYSIS

For wearable applications, the SAR value is a critical parameter. To ensure safety regulations for wearers, the SAR is calculated based on US and European standards. The US standard sets a limit of 1.6 W/kg for 1-g average mass and the European standard sets a limit of 2 W/kg for 10-g average mass. The simulated input power is set to 100 mW. The simulated SARs for the US and European standards are shown in Fig. 16. The simulated SARs at 2.45, 3.0, and 3.45 GHz are 0.29, 0.2, and 0.22 W/kg for the US standard. Meanwhile, for the European standard, the calculated SARs are 0.13, 0.09, and 0.09 W/kg. The simulated SARs for both standards are significantly lower than the limit standards.

In order to meet the safety level of SAR for US and European standards, the maximum of input powers to the antenna should be evaluated. As well known that the SAR value is linearly proportional to the input power. Therefore, the maximum allowable input power for US and European standards can be calculated based on the limit of SAR values and the simulated greatest SAR value at input power of 100 mW as following: $P_m(\text{mW}) = \frac{Limit\text{SAR}value}{GreatestSAR} \times 100$. As a result, the maximum of input power for US standard can be calculated: $P_{US.m} = \frac{1.6}{0.29} \times 100 \approx 550$ mW. Similarly, the maximum of input power for European standard is approximately calculated: $P_{Eur.m} = \frac{2.0}{0.13} \times 100 \approx 1500$ mW. The calculated maximum allowable input power for US and European standards are 550 and 1500 mW, which is far excess for low-power wearable electronic devices.

The comparisons of the proposed antenna with other triple-band wearable antennas are summarized in Table 2. In terms of the antenna size, the antenna in [18] achieves smallest overall size. However, its operating bandwidth is relatively small. The antenna in [17] yields triple-wideband, but antenna gain, efficiency, and SAR are not detail mentioned. In general, the proposed antenna yields adequate triple-band with higher gain, high radiation efficiency with a significantly lower SAR. Thanks to the large conductive textile, it works as a reflector or protective shield to increase antenna gain and reduce the proximity effect, hence minimizing the SAR.

IV. CONCLUSION

This paper presents a wearable triple-band open-ring antenna for 2.45/3.0/3.45 GHz for ISM, military, and WiMAX applications, respectively. The proposed antenna structure is comprised of two substrates: a rigid substrate and a textile substrate. The two open-ring radiators and a 1 by 2 feeding network are printed on the rigid substrate. In addition, a conductive textile ground is attached on the textile substrate. The triple-band open-ring antenna yields directional radiation with high-gain, high-efficiency and a significantly low SAR. The proposed antenna is validated by measurement in free space and in human/phantom body environments showing very good agreement. The experimental results indicate that the proposed antenna is a suitable candidate for off-body communication.

REFERENCES

[1] U. Ullah, I. B. Mabrouk, and S. Koziel, "A compact circularly polarized antenna with directional pattern for wearable off-body communications," *IEEE Antennas Wireless Propag. Lett.*, vol. 18, no. 12, pp. 2523–2527, Dec. 2019.

[2] M. El Atrash, M. A. Abdalla, and H. M. Elhennawy, "Gain enhancement of a compact thin flexible reflector-based asymmetric meander line antenna with low SAR," *IET Microw., Antennas Propag.*, vol. 13, no. 6, pp. 827–832, May 2019.

[3] X. Hu, S. Yan, and G. A. E. Vandenbosch, "Compact circularly polarized wearable button antenna with broadside pattern for U-NII worldwide band applications," *IEEE Trans. Antennas Propag.*, vol. 67, no. 2, pp. 1341–1345, Feb. 2019.

[4] H.-R. Zu, B. Wu, Y.-H. Zhang, Y.-T. Zhao, R.-G. Song, and D.-P. He, "Circularly polarized wearable antenna with low profile and low specific absorption rate using highly conductive graphene film," *IEEE Antennas Wireless Propag. Lett.*, vol. 19, no. 12, pp. 2354–2358, Dec. 2020.

[5] I. Martinez, C.-X. Mao, D. Vital, H. Shahariar, D. H. Werner, J. S. Jur, and S. Bhardwaj, "Compact, low-profile and robust textile antennas with improved bandwidth for easy garment integration," *IEEE Access*, vol. 8, pp. 77490–77500, 2020.

[6] A. Y. I. Ashyap, S. H. B. Dahlan, Z. Z. Abidin, M. H. Dahri, H. A. Majid, M. R. Kamarudin, S. K. Yee, M. H. Jamaluddin, A. Alomainy, and Q. H. Abbasi, "Robust and efficient integrated antenna with EBG-DGS enabled wide bandwidth for wearable medical device applications," *IEEE Access*, vol. 8, pp. 56346–56358, 2020.

[7] M. E. Lajevardi and M. Kamyab, "Ultraminiaturized metamaterial-inspired SIW textile antenna for off-body applications," *IEEE Antennas Wireless Propag. Lett.*, vol. 16, pp. 3155–3158, 2017.

[8] A. K. Biswas and U. Chakraborty, "Compact wearable MIMO antenna with improved port isolation for ultra-wideband applications," *IET Microw., Antennas Propag.*, vol. 13, no. 4, pp. 498–504, Feb. 2019.

[9] S. R. Zahran, M. A. Abdalla, and A. Gaafar, "New thin wide-band bracelet-like antenna with low SAR for on-arm WBAN applications," *IET Microw., Antennas Propag.*, vol. 13, no. 8, pp. 1219–1225, 2019.

[10] G.-P. Gao, C. Yang, B. Hu, R.-F. Zhang, and S.-F. Wang, "A wearable PIFA with an all-textile metasurface for 5 GHz WBAN applications," *IEEE Antennas Wireless Propag. Lett.*, vol. 18, no. 2, pp. 288–292, Feb. 2019.
[11] G.-P. Gao, C. Yang, B. Hu, R.-F. Zhang, and S.-F. Wang, "A wide-bandwidth wearable all-textile PIFA with dual resonance modes for 5 GHz WLAN applications," *IEEE Trans. Antennas Propag.*, vol. 67, no. 6, pp. 4206–4211, Jun. 2019.
[12] K. Zhang, G. A. E. Vandenbosch, and S. Yan, "A novel design approach for compact wearable antennas based on metasurfaces," *IEEE Trans. Biomed. Circuits Syst.*, vol. 14, no. 4, pp. 918–927, Aug. 2020.
[13] M. El Atrash, M. A. Abdalla, and H. M. Elhennawy, "A wearable dual-band low profile high gain low SAR antenna AMC-backed for WBAN applications," *IEEE Trans. Antennas Propag.*, vol. 67, no. 10, pp. 6378–6388, Oct. 2019.
[14] X.-Q. Zhu, Y.-X. Guo, and W. Wu, "A compact dual-band antenna for wireless body-area network applications," *IEEE Antennas Wireless Propag. Lett.*, vol. 15, pp. 98–101, 2016.
[15] M. N. Shakib, M. Moghavvemi, and W. N. L. Binti Wan Mahadi, "Design of a tri-band off-body antenna for WBAN communication," *IEEE Antennas Wireless Propag. Lett.*, vol. 16, pp. 210–213, Feb. 2017.
[16] B. Mandal and S. K. Parui, "Wearable tri-band SIW based antenna on leather substrate," *Electron. Lett.*, vol. 51, no. 20, pp. 1563–1564, Oct. 2015.
[17] A. Yadav, V. K. Singh, P. Yadav, A. K. Beliya, A. K. Bhoi, and P. Barsocchi, "Design of circularly polarized triple-band wearable textile antenna with safe low SAR for human health," *Electronics*, vol. 9, no. 9, pp. 1–12, Aug. 2020.
[18] P. Sambandam, M. Kanagasabai, R. Natarajan, M. G. N. Alsath, and S. Palaniswamy, "Miniaturized button-like WBAN antenna for off-body communication," *IEEE Trans. Antennas Propag.*, vol. 68, no. 7, pp. 5228–5235, Jul. 2020.
[19] S. Mohammadi-Asl, J. Nourinia, C. Ghobadi, and M. Majidzadeh, "Wide-band compact circularly polarized sequentially rotated array antenna with sequential-phase feed network," *IEEE Antennas Wireless Propag. Lett.*, vol. 16, pp. 3176–3179, 2017.
[20] S. I. Latif and L. Shafai, "Polarization characteristics of multiband loaded microstrip annular ring antennas," *IEEE Trans. Antennas Propag.*, vol. 57, no. 9, pp. 2788–2793, Sep. 2009.
[21] T. T. Le, H. H. Tran, and H. C. Park, "Simple-structured dual-slot broadband circularly polarized antenna," *IEEE Antennas Wireless Propag. Lett.*, vol. 17, no. 3, pp. 476–479, Mar. 2018.
[22] T.-A. Le Trong, S. I. H. Shah, G. Shin, S. M. Radha, and I.-J. Yoon, "A compact triple-band antenna with a broadside radiation characteristic for head-implantable wireless communications," *IEEE Antennas Wireless Propag. Lett.*, vol. 20, no. 6, pp. 958–962, Jun. 2021.

TU TUAN LE received the B.S. degree in electronics and telecommunications from Hanoi University of Science and Technology, Hanoi, Vietnam, in 2013, and the Ph.D. degree from the Department of Electronics and Electrical engineering, Dongguk University, Seoul, South Korea. He is currently with Hanyang University, Seoul, as a Postdoctoral Research Fellow. His current research interests include RF energy harvesting, wearable antennas, circularly polarized antennas, reconfigurable antennas, and multiband/broadband planar antennas for various wireless applications.

YONG-DEOK KIM received the B.S. degree in information and communication engineering from Hoseo University, South Korea, in 2020. He is currently pursuing the Ph.D. degree with the Department of Electronics Engineering, Hanyang University, Seoul, South Korea. His current research interests include circularly polarized antennas, wearable antennas, multiband antennas, and on-chip antennas for various wireless applications.

TAE-YEOUL YUN (Member, IEEE) received the Ph.D. degree from the Department of Electrical Engineering, Texas A&M University, College Station, TX, USA, in 2001. From 1989 to 1996, he worked with the Optical Telecommunication System Group, ETRI, Daejon, South Korea, where he developed 2.5- and 10-Gb/s systems. From 2001 to 2003, he was an MMIC Designer at Triquint Semiconductor, Dallas, TX, USA. Since 2003, he has been a Professor at Hanyang University, Seoul, South Korea. His research interests include RFICs, antennas, and wireless/optical high-speed communication systems.